applied sciences

MDPI

Article

A Radial Flow Contactor for Ambient Air CO_2 Capture

Qian Yu and Wim Brilman *

Sustainable Process Technology, Fac. Science & Technology, University of Twente, 7500 AE Enschede, The Netherlands; qianyu1102@googlemail.com
* Correspondence: d.w.f.brilman@utwente.nl

Received: 29 December 2019; Accepted: 22 January 2020; Published: 6 February 2020

Featured Application: Direct Air Capture for microalgae cultivation, horticulture, and solar fuels.

Abstract: Direct air capture (DAC) of CO_2 can address CO_2 emissions from distributed sources and produce CO_2 from air virtually anywhere that it is needed. In this paper, the performance of a new radial flow reactor (RFR) for CO_2 adsorption from ambient air is reported. The reactor uses a supported amine sorbent and is operated in a batch mode of operation or semi-continuously, respectively without or with sorbent circulation. The radial flow reactor, containing 2 kg of the adsorbent, is successfully scaled up from the experimental results obtained with a fixed bed reactor using only 1 g of the adsorbent. In the batch operation mode, the sorbent in the annular space of the RFR is regenerated in situ. With sorbent circulation, the RFR is loaded and unloaded batchwise and only used as an adsorber. A sorbent batch loaded with CO_2 is transported to and regenerated in an external (fluid bed) regenerator. The RFR unit is characterized by a low contacting energy (0.7–1.5 GJ/ton-CO_2) and a relatively short adsorption time (24–43 min) compared to other DAC processes using the same types of sorbents. The contactor concept is ready for further scale-up and continuous application.

Keywords: CO_2; air capture; adsorption; supported amine sorbents; radial flow reactor

1. Introduction

The capture of CO_2 from ambient air, often called direct air capture (DAC), can address anthropogenic CO_2 emissions from distributed sources, which account for between one third and one half of the total CO_2 emissions per year [1]. Unlike CO_2 capture from point sources, DAC facilities can be installed anywhere, providing more flexibility in the choice of location. The captured atmospheric CO_2 can be stored underground or converted to produce fuels and value-added chemicals, such as carbon monoxide, formic acid, and methanol [2–4]. Additionally, the CO_2 can be utilized in biological conversion, e.g., in horticulture or for use in microalgae cultivation [5].

DAC was first suggested by [6] using an aqueous alkali hydroxide solution and was studied on a process level by Baciocchi et al. [7]. An important issue when using aqueous systems for direct air capture is that the required massive air flow may cause significant water losses for the aqueous alkali solution [8]. Essentially the same system was further developed by Keith et al. and was comprised of absorption in an alkaline solution and was coupled to a calcium caustic recovery loop, requiring a temperature of 900 °C during regeneration [9]. Despite its complexity, this optimized and fully engineered system can be regarded as state of the art; it claims to be able to produce CO_2 from air at relatively low costs of 94 USD/ton of CO_2 [10].

Supported amine solid sorbents are a promising alternative for DAC, also at lower production scales, as they need lower regeneration temperatures and avoid evaporative solvent losses. Supported amine sorbents were firstly studied for DAC by Belmabkhout et al. [11], and an increasing number of papers have been published using these sorbents since then [11–23]. Most of the DAC studies target the development of new supported amine sorbents, thereby focusing on enhancing the CO_2 equilibrium capacity, utilizing thermogravimetric analyzers or fixed bed reactors with a few grams of sorbent [24–28]. Studies focusing on the subsequent process development issues, especially at a scale of several kilograms of sorbent, as well as studies reporting on the sorbent performance under non-equilibrium conditions are rare.

Whereas the desorption step more closely resembles the situation encountered in CO_2 capture from concentrated sources, the DAC adsorption step is especially challenging. During adsorption, at least 1400 m^3 of air need to be supplied to capture 1 kg of CO_2 (when the CO_2 concentration in the air at 25 °C is 0.04%). The counteracting requirements of a high gas throughput and, for process economics, low pressure drop lead to the need for the development, testing, characterization, and evaluation of new DAC air–sorbent contactors.

The objective of this paper is to communicate the rationale for selecting a radial flow reactor for this application and to report on an experimental study investigating the suitability of this contactor type for the adsorption step in DAC. In this study, a polymer-based supported amine sorbent will be used for the reversible CO_2 capture process.

Firstly, the general requirements for a sorbent-based DAC contactor are summarized, which led to the selection of a radial flow reactor (RFR) as a potentially attractive contactor type. Considering the large gas volumes to be treated in the DAC adsorber, it is essential to have (i) a high volumetric adsorption rate (in mol CO_2 m^{-3} s^{-1}) to minimize equipment sizes and costs (CapEx) and (ii) a low pressure drop to minimize operational costs (OpEx). Since the energy consumption (with associated emissions) and the operational costs depend linearly on pressure drop and the volumetric flowrate, the efficiency of CO_2 removal is also important.

With these requirements in mind, different contacting methods were evaluated, all based on forced convective flow. The results are presented in Appendix A, Figure A2. It was found that the CO_2 sorbents were saturated much faster and with a much higher removal efficiency—in a classical (axial) fixed-bed contactor and in a fluidized bed—when compared with the use of a parallel-flow fixed bed, which (on its turn) displays a much lower pressure drop. The faster loading rate allows for more cycles per day and hence increased productivity and lower CapEx. Moreover, a fixed-bed reactor seems better suited than a fluidized-bed reactor for capturing CO_2 from air because of the possibility of operating at a lower pressure drop and allowing for a more compact design. A fluidized bed requires not only a gas distributor (with an additional pressure drop) to ensure an even gas distribution, but also a freeboard zone for gas–solid separation. Additionally, fluid beds have a lower contacting efficiency due to bubble formation.

In selecting the operating conditions, the selection of the gas over sorbent ratio (GSR) and the adsorption process time is important, but not straightforward. For the first one, there is a trade-off between the CO_2 supply (sufficient CO_2 supply requires a high air flow rate) and the pressure drop (low pressure drop requires a low air flow rate). The selection of the adsorption time is finding the best trade-off between the gas capture efficiency and the solid conversion (also called sorbent saturation efficiency). A high gas capture efficiency corresponds with high reaction rates, normally found at low sorbent saturations at short adsorption times. A high sorbent saturation efficiency requires a long adsorption time, resulting in a lower system productivity, as the loading rate typically decreases with loading, but a lower energy penalty per kg of CO_2 for sorbent heating during sorbent regeneration.

To represent the GSR, here, we use a parameter called the stoichiometric time. This parameter represents the general mass balance and is defined by the following expression:

$$t_{sto} = \frac{m_S \cdot q_{max}}{\varphi_v \cdot \rho_{CO2}}. \quad (1)$$

Here, m_s (kg) represents the mass of the sorbent, q_{max} (in g CO_2 per kg sorbent) represents the maximum CO_2 amount adsorbed by the sorbent, φ_v (m^3 s^{-1}) represents the volumetric flow of gas introduced to the reactor, and ρ_{CO2} (g m^{-3}) represents the concentration of CO_2 in the gas entering the reactor. Equation (1) shows that parameter t_{sto} is inversely proportional to the GSR. Earlier work showed that the optimal stoichiometric time for CO_2 air capture using the sorbent used in this study is in the range of 15–45 min, with the optimal adsorption time being equal to 0.5–1.5 times the stochiometric time t_{sto} [29]. The experimental data supporting those findings were firstly obtained from a fixed-bed reactor with 1–3 g of sorbent. Then, those optimal operating conditions were derived based on a total cost analysis considering the contacting energy, the regeneration energy, and the sorbent cost [29].

With the fixed-bed type as the optimal contacting method as well as the proper operating conditions, the next step is to select an adsorber to scale up the process to a scale of several kilograms of sorbent. A traditional scale-up of the axially-fixed-bed reactor used for the 1–3 g scale would result in a 'pancake-shaped' flat-bed contactor due to the low pressure drop requirement, occupying a large footprint area and giving rise to difficulties in proper feed gas distribution. In this respect, a radial flow reactor (RFR) was considered to be a good option.

Radial flow reactors were introduced and developed for large-scale chemical plants in the late 1960s and early 1970s [30]. In a radial flow reactor, the sorbent is packed in a coaxial cylindrical annulus and divides the contactor into two gas chambers; one part is called the center pipe and the other one is called the annular channel. In a radial flow reactor, the gas phase passes through the sorbent bed in the radial direction. Note that the small-scale fixed bed is essentially a representative unit cell for the gas phase passing the sorbent in a radial flow reactor. A radial flow reactor can be easily scaled up without significantly increasing the footprint, as it merely needs to increase the height of the cylindrical shape of the reactor instead of its diameter. The configurations of the RFR can be divided into z-type and π-type configurations according to the direction of the inflow and outflow. A z-type RFR has the gas inflow and outflow in the same direction, whereas the inflow and outflow in a π-type RFR are in opposite directions. A π-type RFR is chosen in this study because it has a more uniform flow distribution than that of the z-type [31]. Figure 1 shows the configurations of the reactor types mentioned above.

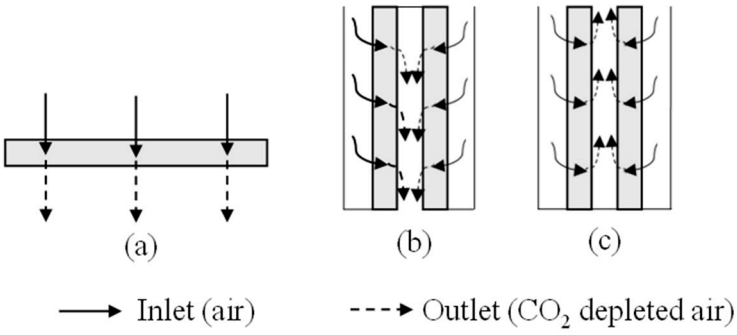

Figure 1. Configurations for (**a**) a flat-bed reactor (**b**) a z-type radial flow reactor (RFR), and (**c**) a π-type RFR.

At present, RFRs have not been investigated for the application of CO_2 direct air capture. In the past two decades, RFRs were studied in some research papers and patents for, e.g., (1) configurations for a uniform flow distribution [31–33], (2) the application of catalytic reactions to produce naphtha [34,35], xylenes [36], methanol [37], or hydrogen [38], and (3) the application of air purification (prior to the cryogenic air separation unit) [39]. No other studies evaluated RFRs for DAC using a supported amine sorbent. Kulkarni et al. estimated the operational cost by modeling the economic performance of a DAC process in a monolithic contactor unit coated with amino-modified silica adsorbent [40]. Brilman and Veneman estimated for a plate-type adsorber on the basis of experimental data in a lab-scale fixed-bed reactor (17 mm in diameter, 50 cm in length) using a supported amine sorbent, resulting in a total cost a total cost of 150–200 USD/ton CO_2 [13]. Zhang et al. evaluated air capture using 1 kg of

polyethylenimine (PEI)-silica sorbent in a bubbling fluidized bed. On the basis of their experimental results, a conceptual design for CO_2 air capture was proposed, for which the operating cost was estimated to be 152 USD/t-CO_2 [41]. In addition to that, Sakwa-Novak et al. evaluated a small-scale monolithic cylinder (2.5 cm in diameter, 10.2 cm in length), impregnated with PEI and suggested an operating cost of 100 USD/t-CO_2 [23].

In this paper, we focus on the process development in the application of CO_2 direct air capture in a radial flow reactor (RFR) using a commercial supported amine sorbent, Lewatit VP OC 1065 (Lewatit), in short: the RFL process (RFR reactor with Lewatit VPOC 1065 as adsorbent). The RFL process is operated at a sorbent scale of 2 km; this is the first time that such a reactor type and such a scale of the sorbent are investigated for the application of CO_2 air capture.

The aim of this paper is an experimental feasibility study of the RFL process. Next to design validation, the RFR is operated as fixed-bed and as (intermittently and continuously) operating moving-bed. The RFL process performance is compared with other sorbents and processes for DAC, indicating that the RFL process is an attractive technology for capturing CO_2 directly from ambient air.

2. Materials and Methods

2.1. Material

The adsorbent used in this study is a supported amine sorbent called Lewatit® VP OC 1065 (Lewatit), manufactured by Lanxess (Germany). This sorbent is a polymeric sorbent that contains primary benzylamine groups as the functional unit [42]. The total nitrogen loading measured by elemental analysis is 6.8 mol/kg [43]. The sorbent is a bead-like material with a diameter between 0.3 and 1 mm, which displays an internal porous structure with an averaged surface area, pore volume, and pore size of 25 m^2/g, 0.20 cm^3/g, and 38 nm, respectively [43]. Packing density for the dry, unloaded material is around 530 kg/m^3.

This sorbent was selected for this study because of its good working capacity and commercial availability in large quantities. The capacity measured in dry air at 25 °C is 1.1 mol/kg. This capacity correlates to an amine efficiency of 16%, which is comparable to the other supported amine sorbents measured by other researchers [44,45] at comparable conditions. The sorbent capacity was found to be stable over the duration of the experimental campaign (one month) as well as over 350 adsorption/desorption cycles under the flue gas conditions [43,46]. The adsorption rate for Lewatit in comparison to other supported amine sorbents under CO_2 air capture conditions is discussed in Section 4.

2.2. Radial Flow Reactor Design

The RFR was designed based on previous results obtained using a fixed-bed reactor (FB) with a sorbent mass of 1–3 g [29]. From those experiments, we found out that the feed rate and external mass transfer do not affect the CO_2 adsorption rate when t_{sto} is 43 min. At this condition (t_{sto} = 43 min), the results showed an overlap of the adsorption rates for the experiments (at 25 °C, 400 ppm CO_2) when using 1, 2, and 3 g of sorbent (the feed gas rate was adjusted according to the change in the sorbent mass) using the fixed-bed reactor. This experimental result was used as the design basis to scale up the process to the kilogram sorbent scale in a radial flow reactor. The results of the RFL process will be compared to these fixed-bed-Lewatit (FBL) data used for the design and are presented in Section 3.2.

The radial flow reactor is designed for the same stoichiometric time as the one used in the FB. The optimal adsorption time was found to be 0.5–1.5 times the stoichiometric time. For the design of the RFL process, this was adopted, aiming for the RFL design to have the same saturation efficiency, CO_2 capacity, and gas residence time as in the FBL experiment.

Specifically, the equivalent gas residence time used in this study is important. This contact time, calculated using the total volume of the sorbent bed (m^3) over the volumetric flow rate of the feeding gas (m^3/s), is preferably small to minimize the contactor volume and to minimize the risk of supply

limitation. Under supply limitations, the rate of sorbent loading is fully determined by the CO_2 supply to the contactor. For the design, a gas residence time of 0.1 s was chosen on the basis of the FB experiments. This contact time is, to the best of our knowledge, the shortest one reported in studies so far [41,47]. More details on the procedures for the RFR design have been presented previously [29].

An inside view of the RFR is shown in Figure A3 in the Appendix A. The internal and external diameters of the sorbent-packing bed are 154 and 184 mm. The sorbent can be filled from the tubes with a diameter of 20 mm located at the top and emptied from the ball valve at the bottom. The external diameter and height of the reactor are 300 and 585 mm. The sorbent is located axially between two wire meshes ordered from Wire Weaving Dinxperlo (the Netherlands). The height of the sorbent-packing bed is 0.4 m. The porosity of the wire mesh itself is 0.48, which was calculated by Matlab based on a photo taken using a high-speed camera from eScope DP-M01.

Figure 2 shows a photo of the RFR and its schematic diagram. The experiment started with desorption by heating the sorbent bed in a flow of nitrogen. To obtain lean sorbent, desorption stopped when the CO_2 outlet concentration was below 10 ppm. In the subsequent adsorption step, ambient air from the surrounding was supplied to the system by a fan (ER 120, Itho Daalderop, The Netherlands). The speed of the fan was controlled by an ABB ACS 150 drive. The volumetric flow of the air supply was measured by a flowmeter from Elster Instromet (Germany). Two CO_2 analyzers (LI-COR LI840A) were used to monitor the CO_2 concentration at the inlet and the outlet (detection range: 0–20,000 ppm; error < 1% of reading). Both analyzers were calibrated just in advance of the first measurement at exactly the same conditions. Four thermocouples were connected to the set-up that measured the temperature of the air supply and the temperature at the top (36 cm), middle (21 cm), and bottom (4 cm) of the bed. To measure the pressure difference between the annular channel and center pipe, a differential pressure transmitter DMD 341 from BD SENSORS (Germany) was utilized; it was connected with two metal tubes whose heights were adjustable. A detailed look at the pressure difference measurement can be found in Figure A4 in Appendix A. During the experiment, the values of the CO_2 concentration at the inlet and outlet, the values of the temperatures, and the pressure difference were recorded every second. The working conditions during testing are listed in Table 1. Note that the CO_2 concentrations vary (and differ from the outdoor), as the unit is located within a process hall.

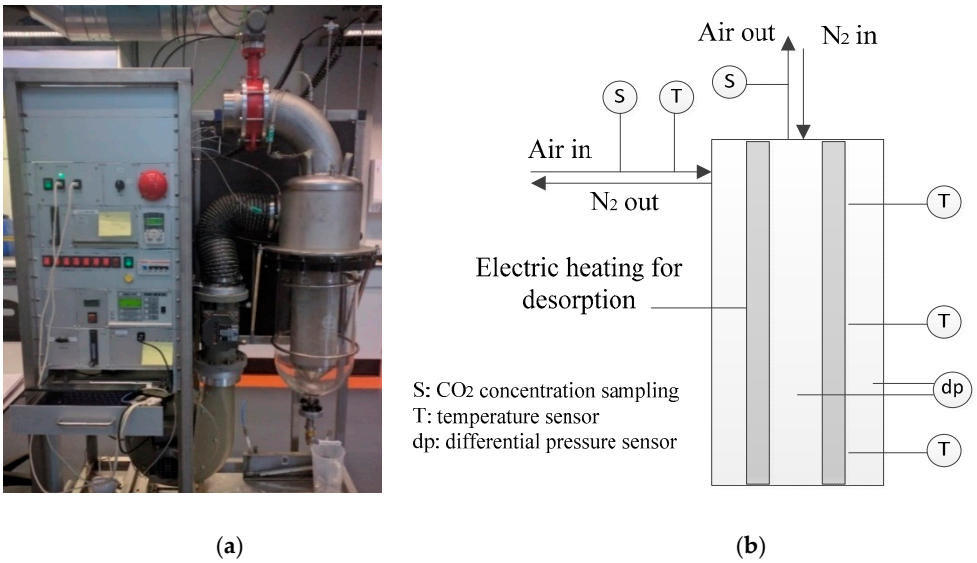

Figure 2. (**a**) Photo; (**b**) Schematic diagram of the radial flow reactor.

Apart from a fixed-bed RFL, operating the RFR as intermittently and continuously moving bed was studied. To test the feasibility of realizing a continuous moving bed inside the RFR, some modifications to the set-up were made. A sorbent container and a rotary valve were added at the

top and at the bottom of the adsorber, respectively. The sorbent container (max. capacity of 2.5 kg of sorbent) was used to feed the RFR with a sufficient and continuous sorbent feed flow. The calibrated rotary valve at the bottom outlet of the reactor was operated at various solid rates (g/s) to realize different sorbent residence times. By operating the rotary valve at various rates (g/s), different sorbent residence times can be realized. A specific view of the moving-bed RFR can be found in Figure A5 in Appendix A. The experimental conditions for the moving-bed RFR are listed in Table 2. During the experiment, initially, the RFR was filled with 1.7 kg of lean sorbent, and an additional 2.4 kg of the lean sorbent was preloaded into the top buffer tank.

Table 1. Working conditions for experimental work for testing RFR in fixed-bed mode.

Adsorption	
Sorbent mass (kg)	1.7
Flow rate (m^3/h)	41–313
CO_2 concentration (ppm)	429–464
Relative humidity (%)	40–65
Temperature (°C)	19–22
Desorption	
Nitrogen purge (m^3/h)	3
Temperature (°C)	120
Duration (h)	16

Table 2. Experimental conditions for the moving-bed RFR tests.

Parameter	**Value**
Sorbent mass in buffer (kg)	2.4
Air flow rate (m^3/h)	188
CO_2 concentration (ppm)	436

3. Results and Discussion

3.1. Pressure Drop

When air flow passes through the RFR, there is a pressure drop between the inflow and the outflow that determines the contacting energy required. This pressure drop is caused by friction with both the sorbent bed and the supporting wire mesh. The pressure differences between the annular gas channel and the center pipe were measured at varying flow rates for both the situations in which the mesh was fully loaded with sorbent and without any sorbent. The pressure drop for a fully loaded bed is between 70 to 700 Pa when the air flow is in the range of 41–313 m^3/h (0.05–0.38 m/s). The maximum pressure drop over the empty RFR (without sorbent) is measured to be (only) 10 Pa, showing that the pressure drop is predominantly caused by the sorbent bed. The results of the aforementioned measurements are shown in Figure A6 in Appendix A.

3.2. Performance of the Fixed-Bed RFL

In this section, experimental work was carried out using a fixed-bed mode of operation for the RFL process, aiming to study the RFR:

1. CO_2 adsorption performance at a larger scale (2 kg) in the RFR in comparison with the results obtained on small scale (1 g) in the FB on which the RFR design is based;
2. CO_2 breakthrough and temperature profiles during a typical CO_2 adsorption test;
3. the rates of CO_2 and water adsorption.

For a fair comparison, the RFR reactor was operated at the same stoichiometric time (t_{sto}) of 43 min as the original FB tests with only 1 g of sorbent. The experimental conditions are listed in

Table 3. Note that although the two reactors were operated at the same t_{sto}, there is a difference of more than 1000 times in parameters such as air flow and sorbent hold up and a difference of 500 times in the geometric aspect ratio of the bed thickness over the contacting area ratio. Furthermore, it is important to note that the experimental determined maximum capacities are different, due to the fact that the FB experiments were carried out with dry, 'synthetic' air of exactly 400 ppm CO_2, whereas the RFR was operated inside the high-pressure laboratory of the University of Twente using the real lab air with 60% relative humidity (RH) and a slightly elevated CO_2 content (here: 452 ppm).

Table 3. Comparison of the experimental conditions in the fixed bed reactor and in the radial flow reactor.

Parameter	Units	Fixed Bed	Radial Flow
Air flow rate	m^3/h	0.072	188
Contacting area	m^2	2.0×10^{-4}	0.23
Aspect ratio (thickness/area)	m/m^2	49.7	0.065
Temperature	°C	25	20
Mass of the sorbent	g	1	1720
CO_2 inlet concentration	ppm	400	452
Stoichiometric time, t_{sto}	min	43	43
Relative humidity, RH	%	0	60
Superficial velocity	m/s	0.1	0.23
Max. working capacity	mol/kg	0.9	1.5

Figure 3 shows the comparison of the two reactors regarding their adsorption performance with respect to the gas capture efficiency (η_G) and the sorbent saturation efficiency (η_s). The first parameter is calculated from the experimentally determined CO_2 concentration in the gas leaving the reactor. using the following equation:

$$\eta_G(t) = \frac{C_{CO2,in} \cdot t - \int_0^t C_{CO2,out} dt}{C_{CO2,in} \cdot t}. \quad (2)$$

The latter is calculated as:

$$\eta_S(t) = \frac{q_t - q_{des}}{q_{eq} - q_{des}}. \quad (3)$$

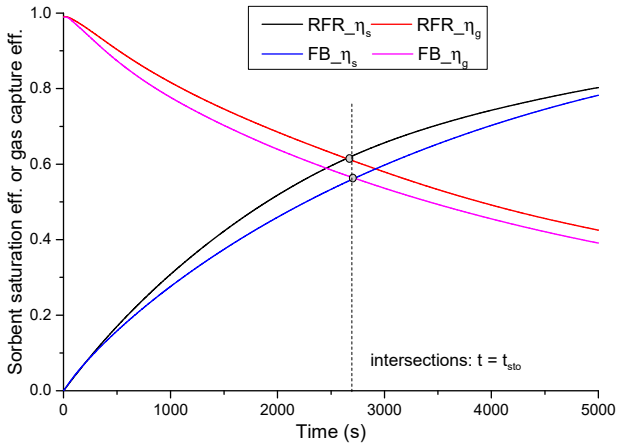

Figure 3. Comparison of the adsorption performance between the RFR and fixed bed (FB) using sorbent saturation efficiency (η_s) and gas capture efficiency (η_G) under the conditions listed in Table 3.

In Equation (2), $C_{CO2,in}$ and $C_{CO2,out}$ represent the concentration of CO_2 in the inlet gas and outlet gas streams of the reactor. In Equation (3), q_t ($g/kg_{sorbent}$) represents the adsorbed CO_2 capacity of the

sorbent at the adsorption time t, q_{eq} is the equilibrium capacity at inlet conditions, and q_{des} represents the residual capacity after desorption.

Figure 3 shows that the variation of the η_s curve and the η_G curve with time are opposite. The intersection points of both curves are found at exactly the stoichiometric time. This finding that η_G equals η_s at the stoichiometric time was presented previously [29].

It can be noticed from Figure 3 that the point where the η_s and η_G curves cross is at a marginally larger value for the RFR due to the variations in temperature, CO_2 concentration, and humidity. The η_s and η_G at $t = t_{sto}$ are 61% for the RFR and 56% for the FB contactor. This limited difference between the RFR and the FB results indicates a successful scale-up, especially considering all of the differences listed in Table 3 and, most importantly, the completely different geometric designs of the two contactors.

The results show once more that the proportional increases of the sorbent amount and the air flow lead to similar efficiencies, despite the large variation of the superficial velocity (0.1 m/s for the FB and 0.23 m/s for the RFR). It also confirms that external mass transfer does not govern the rate of the adsorption process under the studied conditions shown in Figure 3. Hence, the stoichiometric time is found to be a good scale-up criterion for the DAC application, suggesting a predictable η_s curve variation with time. This curve can be used to calculate the working capacity (when q_{eq} is known from the adsorption isotherm) in relation to the choice of the adsorption time. With this, the required sorbent amount can be estimated.

In the design and scale-up of fixed bed processes, three major aspects are typically considered, namely pressure drop, sorbent deactivation, and temperature control (heat effects) [48]. The RFL process shows a relatively low pressure drop (see Section 3.1) which will be compared to other CO_2 air capture processes in Section 4. In addition to that, the adsorbent is stable over at least one month of operation under air capture conditions [43] as well as during 300 h of testing under the flue gas capture [46]. Additionally, in these RFL process tests, we did not find any reduction in the CO_2 working capacity of the adsorbent (see Figure A7). Temperature control and heat effects for the studied RFL process are discussed below.

Figure 4a shows the breakthrough curve and the CO_2 concentration at the inlet for a typical adsorption experiment in RFR. This experiment was operated with the air flow rate of 206 m^3/h, in which the CO_2 concentration varied from 430 to 440 ppm and the RH content is around 40%. In the breakthrough curve, the CO_2 concentration increased immediately after adsorption start-up. The entire breakthrough curve shows a fast adsorption rate in the initial phase and slows down in the subsequent phase. The CO_2 concentration at the outlet reaches 97% of the inflow concentration in the first 2 h at a sorbent capacity of 1.26 mol/kg, but it takes another hour to achieve the maximum capacity (1.33 mol/kg). The studied sorbent was also tested in the gram-scale fixed-bed reactor under the comparable conditions (20 °C, RH 40%, 426 ppm), which demonstrated a similar maximum capacity (1.30 mol/kg).

For the same experiment, the temperature ranged from 19 to 21°C, as illustrated in Figure 4b. Some fluctuations in the temperature of the inflow are observed, which are presumably caused by the varying number of people working in the lab, affecting ventilation rate, inlet temperature, and inlet CO_2 concentration. As a consequence, the temperatures of the sorbent bed change accordingly and those lead to a corresponding change of the CO_2 concentration at the outlet, as shown in Figure 4a. Since the adsorption is an exothermic process, temperature increases lead to less adsorption and thus concentration at the exit increases, whereas temperature decreases lead to the opposite behavior.

In Figure 4b, it is also observed that the three temperatures along the bed are 3–7 °C higher than the inflow temperature in the initial 200 s. This phenomenon is presumably caused by fast water adsorption in the initial phase, as also illustrated in Figure 5. It is observed that the water adsorption is much faster than the CO_2 adsorption, related to its (much) higher concentration in the feed. The H_2O capacity reaches 50% (1.5 mol/kg) of the maximum working capacity (3.0 mol/kg) in the initial 200 s, corresponding to a heat released of 110 kJ, calculated by assuming $\Delta H_{H2O} = 43$ kJ mol^{-1} [49]. Considering that the heat capacity of the sorbent is around 1.5 kJ kg^{-1} K^{-1}, this heat release that

is due to water adsorption is large enough to heat up the sorbent for 7 °C; so, it can well explain the initial temperature rise. Subsequently, the temperatures along the bed stabilize due to slower water adsorption (capacity increases from 1.5 to 2.3 mol/kg between 200 to 400 s). Among the initial temperature rises at the top, middle, and bottom of the bed, the temperature at the top of the bed shows a lower temperature rise because here the bed is more cooled by contact with the large gas inflow to the RFR.

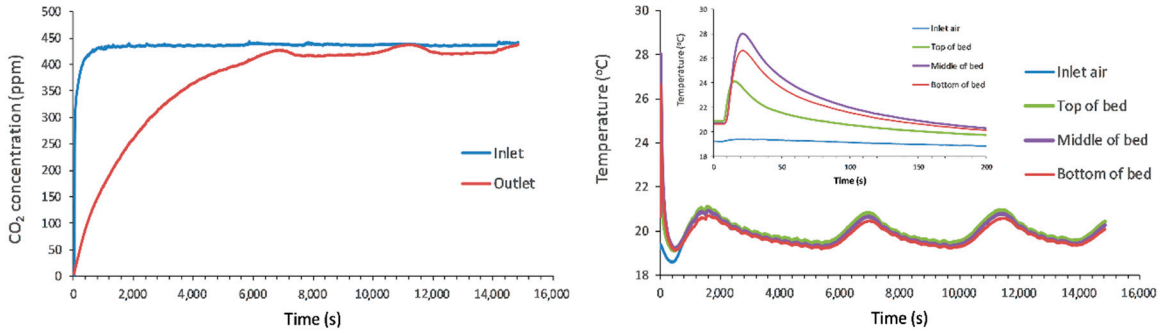

(**a**) (**b**)

Figure 4. (**a**) CO_2 concentration at the inflow (430–440 ppm, 40% RH) and the outflow. (**b**) Temperature profiles during the entire adsorption phase and the initial 200 s (inset).

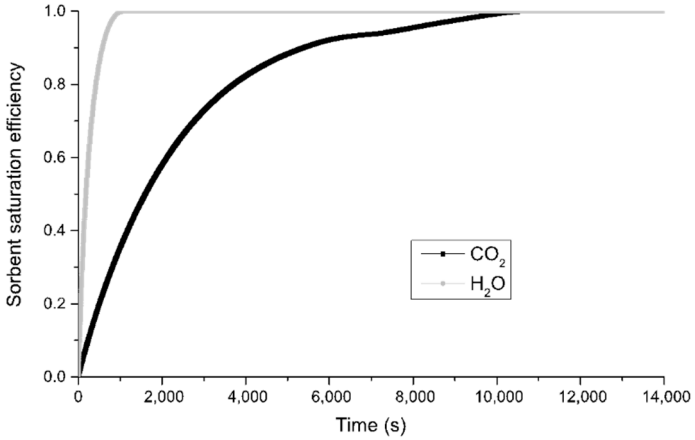

Figure 5. Variation of sorbent saturation efficiency for CO_2 and H_2O with time. Data correspond to the experiment presented in Figure 4.

The air flow rate is an important parameter that determines the adsorption efficiency and economics. We studied the use of different flow rates in the RFR. For each of these runs, the maximum sorbent capacity was determined to check on possible degradation and to check on the mass balance. The results show no effect on the maximum CO_2 capacity with varying flowrate nor with time, implying that the measurement technique with the integration of the analyzer signal is consistent. The data also give an indication of the measurement accuracy and reproducibility. Moreover, the observed patterns between the CO_2 capacity and the inflow CO_2 concentration are very similar. This observation indicates that the minor variation of the CO_2 capacity (as presented in Figure A7 in Appendix A) is a result of the minor variation in the CO_2 inlet concentration (in line with the isotherm) and humidity.

3.3. Checking the Feasibility of a Moving-Bed RFR

A continuous process with sorbent circulation could be advantageous for increasing process productivity and energy consumption, as the process equipment does not need to be heated up or

cooled down every cycle. The objective of the work in this section is to check the feasibility of using a moving-bed RFR with a continuous sorbent flow and to compare its performance (in terms of gas–solid contacting efficiency) with that of using a fixed-bed RFR.

The moving bed was operated under the conditions listed in Table 2. Figure 6 shows the variation of outlet CO_2 concentration with time for both operating modes. The curve for the moving-bed RFR can be separated into three parts. First, there is a 'startup' period in the first 2000 s, where the concentration in the outlet gas flow gradually increases. From around 2000 s to around 4000 s, a steady-state situation with respect to CO_2 adsorption was achieved, with a developed sorbent loading gradient inside the RFR. After 4000 s, there was no available lean sorbent anymore in the top buffer tank, and since the bottom rotary valve kept removing sorbents from the system, the RFR was gradually emptied. At approximately 4500 s, the empty space at the top of the wire mesh in RFR is big enough to let all of the inflow air pass through; therefore, the outflow CO_2 concentration reaches the concentration at the inlet.

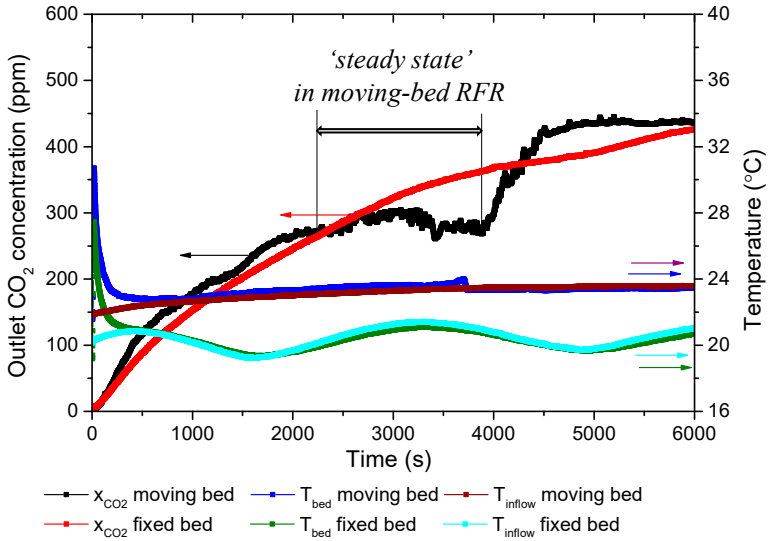

Figure 6. Variation of CO_2 outlet concentration (x_{CO2}), bed temperature (T_{bed}), and inflow temperature (T_{inflow}) with time in the fixed-bed and the moving-bed modes, both operated at the same stoichiometric time (43 min). Conditions are presented in Table 2.

Apart from the outlet CO_2 concentration profile, Figure 6 shows the temperature profiles of both the bed and the inflow. It is observed that the bed temperature of the moving bed is some 3 °C higher than that of the fixed-bed, which can be explained by the variation of the room temperature (referring to T_{inflow} shown in Figure 6). The bed temperature profile shown here refers to the temperature at the middle of the bed. For the moving-bed run, there was a slight step down of the temperature when the top bed became empty at 3600 s. There are initial temperature rises (at $t < 200$ s) for both operating modes, similar to those in Section 3.1, which are attributed to water adsorption. Assuming complete adsorption of incoming water vapor on the sorbent up to the saturation point, the adiabatic temperature rise is calculated to be around 7 °C, matching the experimentally observed temperature excursion. The initial temperature rise in the moving bed displays a similar pattern to the one in the fixed bed, which indicates that the rate of heat generation due to water co-adsorption dominates over any possible improvement in heat transfer in the moving-bed configuration.

The steady-state situation between around 2000 s to around 4000 s indicates the mechanical feasibility of the concept. However, the CO_2 adsorption efficiency found was less promising. From the averaged CO_2 concentration (285 ppm) in this period of steady state, the average loading was calculated and compared to the sorbent loading at the same (average) sorbent adsorption time of 43 min (equal to the operating stoichiometric time). The results show a 46% reduction in working

capacity (from 0.91 to 0.49 mol/kg) as well as a reduction in gas efficiency from 62% to 35% for the moving-bed RFR. The variation of the η_s and the η_G with time for both operating modes can be found in Figure A8 in Appendix A.

Moreover, the phenomena of "cavity" and "pinning" may occur in a moving-bed RFR when the gas flowrate exceeds a certain value. These phenomena may lead to a reduced capture efficiency [50,51]. A "cavity" can be formed between the inflow wall and sorbent, as the drag force between the gas flow and sorbent increases when the gas flow increases. Due to the formation of a cavity, the effective bed length (in the direction of the gas flow) decreases and gas can bypass part of the sorbent bed; further maldistribution of the gas flow may occur. Indeed, we observed some cavities adjacent to the inflow wall. In addition, the sorbent's downward movement was non-uniform. Decreasing the gas flow rate visually avoided the appearance of cavities, but this leads to a lower CO_2 supply rate and a longer effective t_{sto}.

When the gas flow increases further, the gas flow exerts stronger normal stress to the particle, corresponding with an increment in the frictional force between the particle and the outflow wall. The particle will be "pinned" to the wall if the friction force is sufficient to hold the particle weights, and the downward movement of the particle stops. We observed that the "pinning" appeared when the feeding gas flow was further increased beyond 200 m^3/h. The phenomena discussed above make the moving-bed operation practically challenging. More work is needed to investigate whether this can be resolved by modifying the geometry or operating conditions.

The time required to fill and empty the RFR is less than two minutes. In comparison with the adsorption time, this operating time loss (less than 5%) is significantly lower than the loss in working capacity when switching to continuous operation. Considering the above issues, the RFL process will used a fixed-bed RFR intermittently filled with freshly regenerated sorbent and emptied towards the desorber (after sorbent saturation) as the preferred operating method for further study.

4. Discussion

In this section, the RFL process is evaluated using two criteria. The first criterion is the CO_2 adsorption rate per unit volume of the contactor (as an indicator for contactor investment costs) and, secondly, the air–sorbent contacting energy per amount of CO_2 captured (as an indicator for operating energy costs). As the CO_2 adsorption rate is determined by both sorbent properties (such as pore size and volume, particle size, and working capacity) and operating conditions (flow rate and temperature) rather than the reactor type, the adsorption rate of the RFL process is evaluated by comparing with other DAC sorbents published in papers focused on sorbent development. In contrast, the factors for determining the contacting energy are multifaceted, including not only the sorbent property and the operating conditions, but also the reactor type. In this way, the RFL process will be compared with those papers for DAC studying both the sorbent and the reactor.

For the studies on the adsorption rate of the adsorbent, normally the comparison among different sorbents is made by comparing the values of "adsorption half-time" (t_{50}): The time required to reach 50% of the final equilibrium CO_2 capacity [17,52]. However, t_{50} is also dependent on the CO_2 supply rate. The effect of the supply rate on the (observed) adsorption half-time is often not addressed for DAC sorbent screening.

Here, we evaluate the adsorption rate of the sorbent used with those reported in literature at comparable supply rate conditions. For this, the stoichiometric time (t_{sto}) concept is used, introduced in Equation (1), which considers the differences both in the CO_2 supply rate and in the sorbent CO_2 capacity among various sorbents. In this way, a fair comparison of the adsorption rates among different sorbents and processes can be made. In line with most literature studies, adsorption half-time (t_{50}) is used to represent the adsorption rate here. The corresponding minimum time to reach that 50% of q_{max} is 50% of the stoichiometric time for complete sorbent saturation (t_{sto}). Figure 7 shows the t_{50} of the Lewatit sorbent used in this study in comparison to other solid functionalized sorbents tested at air capture conditions from the literature [17,25,47,52]. The operating flows of 188, 206, 273, and

313 m^3/h studied for Lewatit correspond to the 50% t_{sto} values of 22, 18, 16, and 12 min, respectively. Note that other data from the literature listed in Figure 7 were all obtained from experiments at 25 °C. Considering that there is only a 5 °C difference in the adsorption temperature (in this study, measurements are done around 20 °C), the effect of temperature on the adsorption rate among different sorbents is negligible.

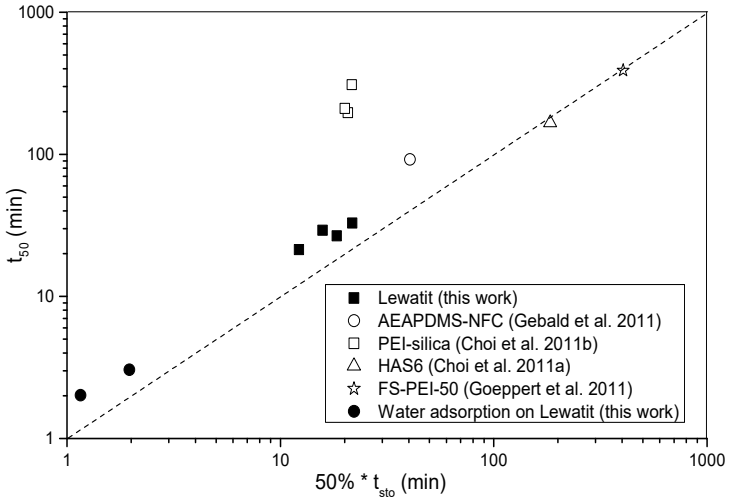

Figure 7. The relationship between the CO_2 and water sorbent saturation half-time (t_{50}) and the stoichiometric time (50% t_{sto}) for Lewatit VP OC 1065 (data: See Figure A7 in Appendix A) compared with those of other air capture sorbents studied by [17,25,47,52].

The 50% t_{sto} values (20–22 min) of various PEI/silica are similar to the one for the studied Lewatit sorbent, tested at φ_v = 188 m^3/h. However, their t_{50} values are much longer than the sorbent used in this study. The reported minimum t_{50} of PEI/silica is 196 min and it is around five times longer than the t_{50} for Lewatit (33 min). Note that the PEI/silica data were measured using a thermogravimetric analyzer (TGA), while other referred adsorbents were tested in fixed beds.

Unlike the comparison with PEI-silica, the comparison of the studied sorbent with AEAPDMS-NFC, HAS6, and FS-PEI-50 is not straightforward due to the large differences in 50% t_{sto}. Because the q_{max} for those sorbents do not differ largely (1.3–1.7 mol/kg), the difference in 50% t_{sto} is due to the large difference in their CO_2 supply rate. Figure 7 shows a dashed parity line, representing t_{50} = 50% t_{sto}. For results that lie on the parity line, their adsorption rates are equal to the supply rates, implying marginal mass transfer and reaction kinetics limitations (in other words: Supply rate limitation). This is the case for HAS6 and FS-PEI-50, which are tested at very slow supply rates. Those supply rates are considered less attractive for practical application because they lead to much longer adsorption times as well as fewer cycle numbers. The adsorption half-time of HAS6 was constrained by mass transfer through the pores due to its morphology characters according to [17]. In comparison, the Lewatit sorbent has larger pores (38 vs. 4.9 nm) and larger pore volume (0.2 vs. 0.11 mL/g) than those for HAS6. From this comparison, we may expect that the adsorption rate for Lewatit will be faster than that for HAS6 in the applied t_{sto} range for Lewatit.

For a relative fast supply rate, like that for both AEAPDMS-NFC and Lewatit, the t_{50} lies above the dashed line, indicating some extents of rate limitation in the mass transfer, the intrinsic reaction, or both. These limitations increase when the supply rate increases. The AEAPDMS-NFC sorbent, tested at a smaller supply rate, already deviates more (in the vertical direction) from the parity line in Figure 7 than the sorbent used in this work. It therefore seems plausible that at comparable supply conditions, in the range of 15–30 minutes for 50% of t_{sto}, this difference will be significantly larger, underlining the fast adsorption rate of the Lewatit sorbent.

Note that the t_{50} values for water adsorption using the studied sorbent and its relation to 50% t_{sto} are also shown in Figure 7. The short t_{sto} values are due to the much higher water content in air compared to CO_2. Those two results for water are in line with the results of CO_2 adsorption using the studied sorbent. This indicates that the water adsorption, shown in Figure 5, is also fast. Overall, it can be summarized that the sorbent used shows a good performance with respect to the adsorption rate for DAC in comparison with other sorbents reported in the literature.

Moving forward to the evaluation of the RFL process regarding the contacting energy, Table 4 shows the comparison of the adsorption characteristics among various DAC systems, all using supported amine sorbents. The results listed for this work are calculated using the data shown in Figure 7. The operating conditions in the present study were selected based on an optimization strategy presented in an earlier study [29]. The conditions for other studies [40,41,53] were taken from the respective studies at conditions selected by the respective authors for their technical/economic assessment. We recalculated the t_{sto} values for these studies, and the results (included in Table 4) show that the conditions in this work (24–43 min) are within the range covered by the references (14–101 min).

Table 4. Comparison of contacting energies for air capture using supported amines—present study compared with selected literature.

Reference	**[41]**	**[40]**	**[53]**	***(This Work)***
Sorbent	PEI-silica	TRI-PE-MCM-41	MIL-101(Cr)-PEI800/ mmen-Mg_2(dobpdc)	Lewatit VP OC 1065
Sorbent type	impregnated	grafted	MOF	Polymeric
Capture system	Circ. Fluid Bed	monolith	monolith	RFR
ΔP adsorber (Pa)	1592	100	n.m.	348-681 [(a)]
t_{sto} (min)	14	101	31/88	24–43
Selected t_{ads} (min)	15	101	19/60	24–43
Contact energy (GJ/t_{CO2})	3.4 [(b)]	0.3 [(c)]	2.3/2.1	0.7–1.5

[(a)] The pressure drop was measured using the applied flow rates for results shown in Figure 7. [(b)] Including 0.4 GJ/tCO_2 for CO_2 compression (efficiency is assumed to be 80%). [(c)] Fan efficiency is assumed to be 80%.

For the selected cases, it is observed that the pressure drop and the electricity consumption for the RFL process are significantly lower than the sorbent circulation process using PEI-silica and a circulating fluidized bed reactor [41]. The process using TRI-PE-MCM-41 in a monolithic contactor possessed the lowest pressure drop in this comparison, but required a longer adsorption time, presumably caused by a long t_{sto} [40]. A longer adsorption time decreases the number of cycles per day and the reactor productivity, and eventually increases the sorbent and the reactor costs. Furthermore, monolithic contactors require time (and energy) for heating/cooling taking place in the same contactor.

The importance of the stoichiometric time in Equation (1) implies at the same time that for changing (weather) conditions affecting the sorbent loading q_{max}, the actual gas velocity should also be adapted by process control. For completeness' sake, it should be mentioned that this work focuses on the DAC adsorption step and not the desorption step, which needs further investigation. The sorbent desorption using hot nitrogen gas, as used in this study, was done solely for the purpose of obtaining lean sorbent. Based on the comparison of sorbent loading kinetics and contactor performance, the studied "RFL DAC" system seems to be a promising option for adsorbing CO_2 from ambient air.

5. Conclusions

In this study, CO_2 capture from ambient air is evaluated for the combination of a novel radial flow reactor and a polymeric supported amine sorbent. The radial flow reactor, containing 2000 g of sorbent, showed a performance in accordance with the design basis. The design was based on fixed-bed experiments using only 1 g of sorbent. This study shows that this radial flow reactor can be

designed and scaled up with confidence based on fixed-bed adsorption data. The studied sorbent is found to have a fair CO_2 capacity and fast adsorption rate. The total RFL system is characterized by a low pressure drop and low contacting energy, uniform flow distribution, short gas residence time, and short adsorption time (24–43 min), making it a good candidate for direct air capture applications and further scale-up.

Author Contributions: Conceptualization and methodology: Q.Y. and W.B.; validation: Q.Y.; writing: Q.Y. and W.B. Supervision. All authors have read and agreed to the published version of the manuscript.

Funding: This research was carried out within the EU MIRACLES project (www.miraclesproject.eu) and has received funding from the European Union's Seventh Framework Program for research, technological development, and demonstration under grant agreement No 613588.

Acknowledgments: Benno Knaken, Johan Agterhorst, and Karst van Bree are acknowledged for their great work in the construction of the set-up.

Conflicts of Interest: The authors declare no conflict of interest.

Appendix A

Selection of the Contacting Method

We selected the gas–solid contacting methods from the parallel-flow fixed bed and the crossflow fixed bed and fluidized bed. The selection was based on the experimental work that was operated in a fixed-bed reactor with an internal diameter (ID) of 1.6 cm and a reactor length of 50 cm. To mimic a parallel-flow gas–solid contacting, a highly porous wire mesh cylinder (ID: 1 cm) was made to hold the sorbent and was placed coaxially at the centerline of the fixed-bed holder. For a fair comparison, the CO_2 adsorption experiments were operated with three different contacting methods under the same conditions. We added 3 g of the sorbent to the reactor, and the experimental work for three different contacting methods was carried out under a gas velocity of 0.4 m/s with 400 ppm CO_2 in the feeding gas (balanced with high-purity N_2) at 25 °C. The minimum fluidization velocity was measured to be 0.1 m/s. The selected gas velocity was almost four times that of the minimum fluidization velocity and was able to achieve a vibrant fluidization. The diagram of the side-view for the three contacting methods is shown in Figure A1.

The experimental results of using different contacting methods are shown in Figure A2. In Figure A2, we use the fractional CO_2 adsorption (instantaneous sorbent capacity q_t over equilibrium sorbent capacity q_e) to represent how fast CO_2 is adsorbed by the sorbent. The results clearly show that the CO_2 adsorption for the parallel-flow fixed bed is much slower than those of the other contacting methods. A slow CO_2 adsorption reduces the reactor productivity (mol CO_2/m^3(reactor)/s) and increases the capital cost. As a result, the parallel-flow fixed bed is discarded.

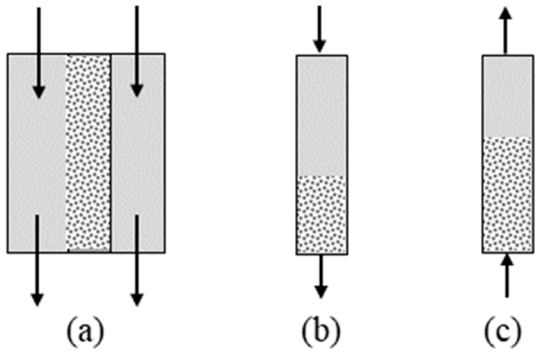

Figure A1. Diagram of the side-view for (**a**) a parallel-flow fixed bed, (**b**) a fixed bed, and (**c**) a fluidized bed.

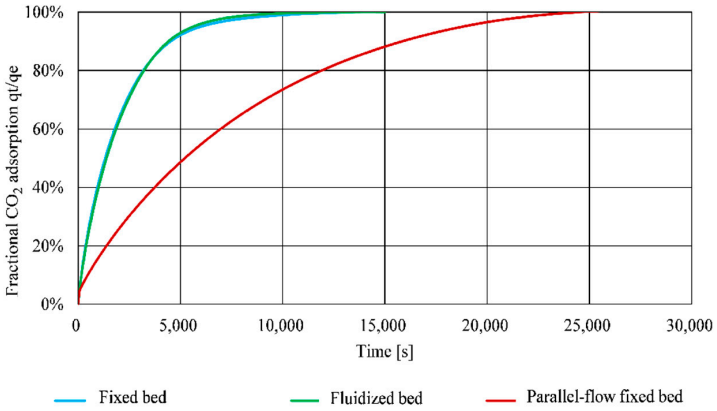

Figure A2. Fractional CO_2 adsorption using different gas-sorbent contacting methods from Figure A1.

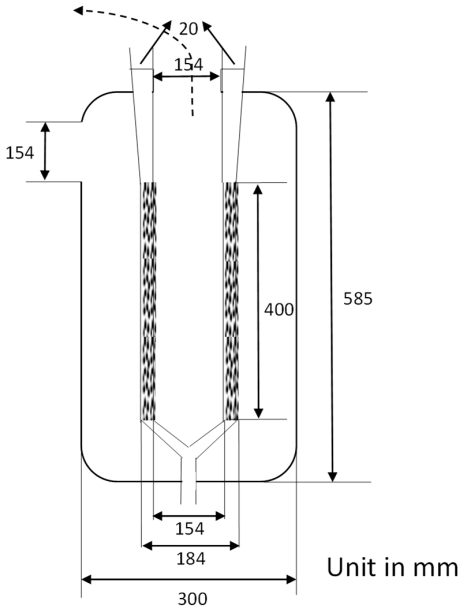

Figure A3. Dimensions of the radial flow reactor.

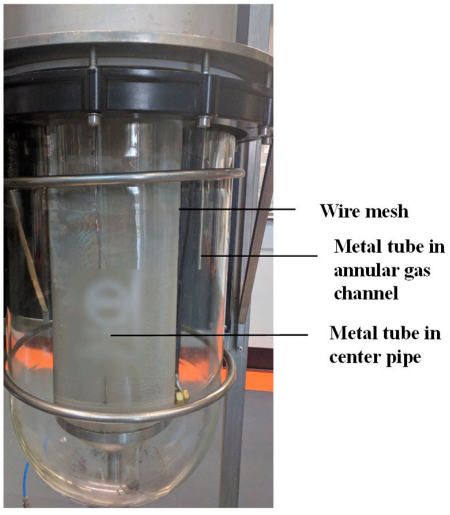

Figure A4. Photo of the zoomed-in look of the RFR.

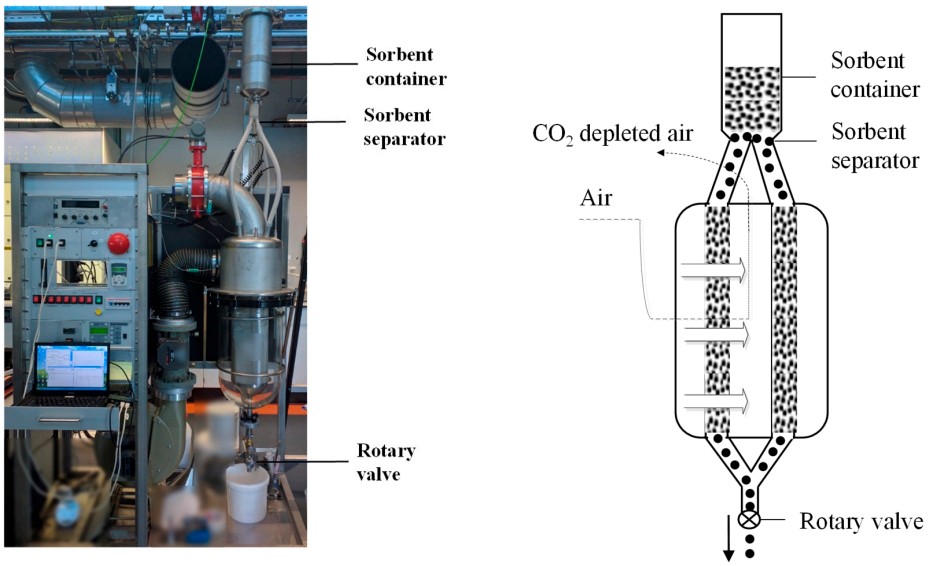

Figure A5. (**a**) Photo; (**b**) Schematic diagram of the modified set-up for testing the moving-bed RFR.

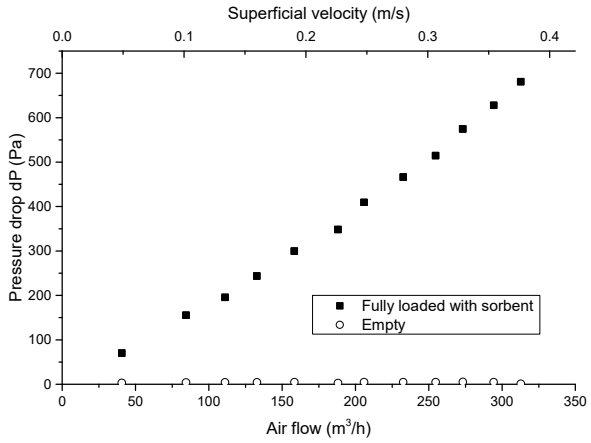

Figure A6. Pressure drop over the RFR unit with a fully sorbent-loaded bed and an empty bed (wire mesh only) at varying flow rates and corresponding superficial velocities.

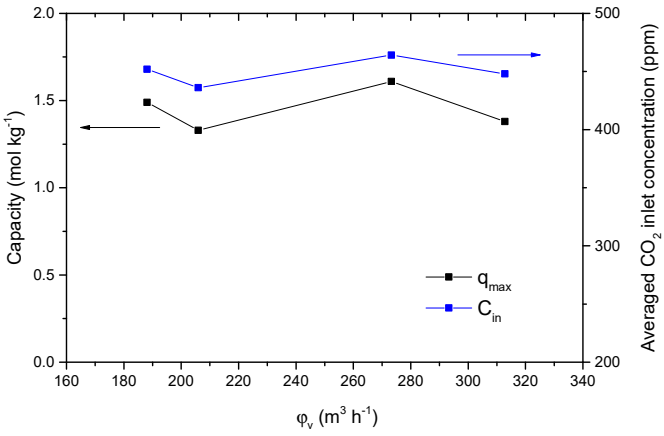

Figure A7. Maximum CO_2 adsorption capacity and average inlet concentration at varying flow rates (T = 20–21 °C, RH = 40%–65%).

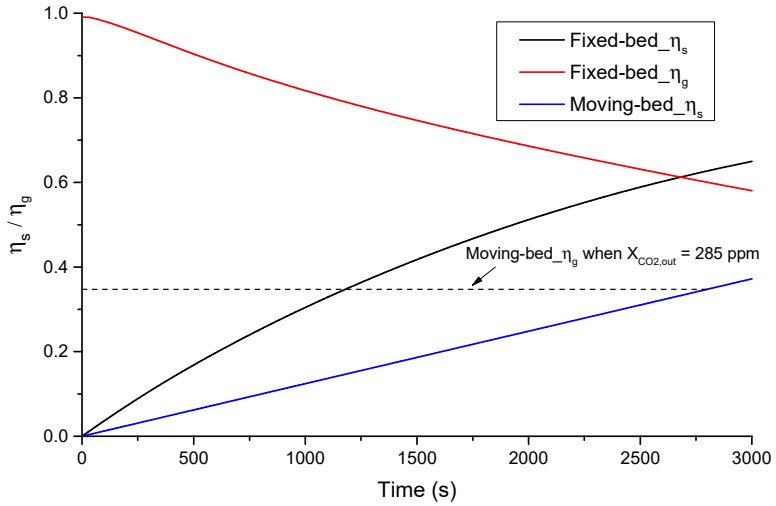

Figure A8. The variation of the η_S and η_G with time for the fixed-bed RFR and moving-bed RFR. (q_{max} = 1.5 mol/kg; xout for moving-bed RFR = 285 ppm).

References

1. Lackner, K.S.; Brennan, S.; Matter, J.M.; Park, A.H.A.; Wright, A.; van der Zwaan, B. The urgency of the development of CO_2 capture from ambient air. *Proc. Natl. Acad. Sci. USA* **2012**, *109*, 13156–13162. [CrossRef] [PubMed]
2. Goeppert, A.; Czaun, M.; Prakash, G.K.S.; Olah, G.A. Air as the renewable carbon source of the future: An overview of CO_2 capture from the atmosphere. *Energy Environ. Sci* **2012**, *5*, 7833–7853. [CrossRef]
3. Graves, C.; Ebbesen, S.D.; Mogensen, M.; Lackner, K.S. Sustainable hydrocarbon fuels by recycling CO_2 and H_2O with renewable or nuclear energy. *Renew. Sust. Energ. Rev* **2011**, *15*, 1–23. [CrossRef]
4. Martens, J.A.; Bogaerts, A.; De Kimpe, N.; Jacobs, P.A.; Marin, G.B.; Rabaey, K.; Saeys, M.; Verhelst, S. The Chemical Route to a Carbon Dioxide Neutral World. *ChemSusChem* **2017**, *10*, 1039–1055. [CrossRef] [PubMed]
5. Sanz-Pérez, E.S.; Murdock, C.R.; Didas, S.A.; Jones, C.W. Direct Capture of CO_2 from Ambient Air. *Chem. Rev.* **2016**, *116*, 11840–11876. [CrossRef] [PubMed]
6. Lackner, K.S.; Ziock, H.-J.; Grimes, P. Carbon capture from air, is it an option? In Proceedings of the 24th Annual Technical Conference on Coal Utilisation and Fuel Systems, Clearwater, FL, USA, 8–11 March 1999.
7. Baciocchi, R.; Storti, G.; Mazzotti, M. Process design and energy requirements for the capture of carbon dioxide from air. *Chem. Eng. Process. Process Intensif.* **2006**, *45*, 1047–1058. [CrossRef]
8. Zeman, F. Energy and material balance of CO_2 capture from ambient air. *Environ. Sci. Technol.* **2007**, *41*, 7558–7563. [CrossRef]
9. Keith, D.W.; Holmes, G.; St. Angelo, D.; Heidel, K. A Process for Capturing CO_2 from the Atmosphere. *Joule* **2018**, *2*, 1573–1594. [CrossRef]
10. Tollefson, J. Price of sucking CO_2 from air plunges. *Nature* **2018**, *558*, 173. [CrossRef]
11. Belmabkhout, Y.; Serna-Guerrero, R.; Sayari, A. Amine-bearing mesoporous silica for CO_2 removal from dry and humid air. *Chem. Eng. Sci.* **2010**, *65*, 3695–3698. [CrossRef]
12. Breault, R.W.; Spenik, J.L.; Shadle, L.J.; Hoffman, J.S.; Gray, M.L.; Panday, R.; Stehle, R.C. Carbon capture test unit design and development using amine-based solid sorbent. *Chem. Eng. Res. Des.* **2016**, *112*, 251–262. [CrossRef]
13. Brilman, D.W.F.; Veneman, R. Capturing atmospheric CO_2 using supported amine sorbents. *Energy Procedia* **2013**, *37*, 6070–6078. [CrossRef]
14. Wang, T.; Lackner, K.S.; Wright, A. Moisture Swing Sorbent for Carbon Dioxide Capture from Ambient Air. *Environ. Sci. Technol.* **2011**, *45*, 6670–6675. [CrossRef]
15. Wang, T.; Hou, C.; Ge, K.; Lackner, K.S.; Shi, X.; Liu, J.; Fang, M.; Luo, Z. Spontaneous Cooling Absorption of CO_2 by a Polymeric Ionic Liquid for Direct Air Capture. *J. Phys. Chem. Lett* **2017**, *8*, 3986–3990. [CrossRef]

16. Wurzbacher, J.A.; Gebald, C.; Brunner, S.; Steinfeld, A. Heat and mass transfer of temperature–vacuum swing desorption for CO_2 capture from air. *Chem. Eng. J.* **2016**, *283*, 1329–1338. [CrossRef]
17. Choi, S.; Drese, J.H.; Eisenberger, P.M.; Jones, C.W. Application of amine-tethered solid sorbents for direct CO_2 capture from the ambient air. *Environ. Sci. Technol.* **2011**, *45*, 2420–2427. [CrossRef]
18. Darunte, L.A.; Oetomo, A.D.; Walton, K.S.; Sholl, D.S.; Jones, C.W. Direct Air Capture of CO_2 Using Amine Functionalized MIL-101(Cr). *ACS Sustain. Chem. Eng.* **2016**, *4*, 5761–5768. [CrossRef]
19. Elfving, J.; Bajamundi, C.; Kauppinen, J.; Sainio, T. Modelling of equilibrium working capacity of PSA, TSA and TVSA processes for CO_2 adsorption under direct air capture conditions. *J CO2 Util.* **2017**, *22*, 270–277. [CrossRef]
20. Gebald, C.; A. Wurzbacher, J.; Borgschulte, A.; Zimmermann, T.; Steinfeld, A. Single-Component and Binary CO_2 and H_2O Adsorption of Amine-Functionalized Cellulose. *Environ. Sci. Technol.* **2014**, *48*, 2497–2504. [CrossRef]
21. Lackner, K.S.; Grimes, P.; Ziock, H.J. Capturing carbon dioxide from air. *Carbon Capture Storage CO_2 Manag. Technol.* **2014**, 364–376.
22. Mutyala, S.; Jonnalagadda, M.; Mitta, H.; Gundeboyina, R. CO_2 capture and adsorption kinetic study of amine-modified MIL-101 (Cr). *Chem. Eng. Res. Des.* **2019**, *143*, 241–248. [CrossRef]
23. Sakwa-Novak, M.A.; Jones, C.W. Steam Induced Structural Changes of a Poly(ethylenimine) Impregnated gamma-Alumina Sorbent for CO_2 Extraction from Ambient Air. *ACS Appl. Mater. Interfaces* **2014**, *6*, 9245–9255. [CrossRef]
24. Sehaqui, H.; Gálvez, M.E.; Becatinni, V.; Cheng Ng, Y.; Steinfeld, A.; Zimmermann, T.; Tingaut, P. Fast and reversible direct CO_2 capture from air onto all-polymer nanofibrillated cellulose-polyethylenimine foams. *Environ. Sci. Technol.* **2015**, *49*. [CrossRef]
25. Goeppert, A.; Czaun, M.; May, R.B.; Prakash, G.K.S.; Olah, G.A.; Narayanan, S.R. Carbon dioxide capture from the air using a polyamine based regenerable solid adsorbent. *J. Am. Chem. Soc.* **2011**, *133*, 20164–20167. [CrossRef]
26. Lu, W.; Sculley, J.P.; Yuan, D.; Krishna, R.; Zhou, H.-C. Carbon Dioxide Capture from Air Using Amine-Grafted Porous Polymer Networks. *J. Phys. Chem. C* **2013**, *117*, 4057–4061. [CrossRef]
27. McDonald, T.M.; Lee, W.R.; Mason, J.A.; Wiers, B.M.; Hong, C.S.; Long, J.R. Capture of Carbon Dioxide from Air and Flue Gas in the Alkylamine-Appended Metal–Organic Framework mmen-Mg_2(dobpdc). *J. Am. Chem. Soc.* **2012**, *134*, 7056–7065. [CrossRef]
28. Sculley, J.P.; Zhou, H.-C. Enhancing Amine-Supported Materials for Ambient Air Capture. *Angew. Chem. Int. Ed.* **2012**, *51*, 12660–12661. [CrossRef]
29. Yu, Q.; Brilman, D.W.F. Design Strategy for CO_2 Adsorption from Ambient Air Using a Supported Amine Based Sorbent in a Fixed Bed Reactor. *Energy Procedia* **2017**, *114*, 6102–6114. [CrossRef]
30. Li, J.C.H. Radial-Flow Packed-Bed Reactors. In *Ullmann's Encyclopedia of Industrial Chemistry*; Wiley: Hoboken, NJ, USA, 2007.
31. Kareeri, A.A.; Zughbi, H.D.; Al-Ali, H.H. Simulation of Flow Distribution in Radial Flow Reactors. *Ind. Eng. Chem. Res.* **2006**, *45*, 2862–2874. [CrossRef]
32. Mu, Z.; Wang, J.; Wang, T.; Jin, Y. Optimum design of radial flow moving-bed reactors based on a mathematical hydrodynamic model. *Chem. Eng. Process. Process Intensif.* **2003**, *42*, 409–417. [CrossRef]
33. Wang, J.; Wang, H. Discrete method for design of flow distribution in manifolds. *Appl. Therm. Eng.* **2015**, *89*, 927–945. [CrossRef]
34. Iranshahi, D.; Rahimpour, M.R.; Asgari, A. A novel dynamic radial-flow, spherical-bed reactor concept for naphtha reforming in the presence of catalyst deactivation. *Int. J. Hydrogen Energy* **2010**, *35*, 6261–6275. [CrossRef]
35. Rahimpour, M.R.; Iranshahi, D.; Pourazadi, E.; Paymooni, K. Evaluation of Optimum Design Parameters and Operating Conditions of Axial- and Radial-Flow Tubular Naphtha Reforming Reactors, Using the Differential Evolution Method, Considering Catalyst Deactivation. *Energy Fuels* **2011**, *25*, 762–772. [CrossRef]
36. Hamedi, N.; Tohidian, T.; Rahimpour, M.R.; Iranshahi, D.; Raeissi, S. Conversion enhancement of heavy reformates into xylenes by optimal design of a novel radial flow packed bed reactor, applying a detailed kinetic model. *Chem. Eng. Res. Des.* **2015**, *95*, 317–336. [CrossRef]
37. Parvasi, P.; Jokar, S.M. A novel reactor configuration for industrial methanol production from the synthesis gas. *J. Energy Resour. Technol. Trans. ASME* **2019**, *141*. [CrossRef]

38. Palma, V.; Palo, E.; Ciambelli, P. Structured catalytic substrates with radial configurations for the intensification of the WGS stage in H_2 production. *Catal. Today* **2009**, *147*, S107–S112. [CrossRef]
39. Tian, Q.; He, G.; Wang, Z.; Cai, D.; Chen, L. A Novel Radial Adsorber with Parallel Layered Beds for Prepurification of Large-Scale Air Separation Units. *Ind. Eng. Chem. Res.* **2015**, *54*, 7502–7515. [CrossRef]
40. Kulkarni, A.R.; Sholl, D.S. Analysis of equilibrium-based TSA processes for direct capture of CO_2 from Air. *Ind. Eng. Chem. Res.* **2012**, *51*, 8631–8645. [CrossRef]
41. Zhang, W.; Liu, H.; Sun, C.; Drage, T.C.; Snape, C.E. Capturing CO_2 from ambient air using a polyethyleneimine-silica adsorbent in fluidized beds. *Chem. Eng. Sci.* **2014**, *116*, 306–316. [CrossRef]
42. Alesi, W.R.; Kitchin, J.R. Evaluation of a primary amine-functionalized ion-exchange resin for CO_2 capture. *Ind. Eng. Chem. Res.* **2012**, *51*, 6907–6915. [CrossRef]
43. Yu, Q.; Delgado, J.D.L.P.; Veneman, R.; Brilman, D.W.F. Stability of a Benzyl Amine Based CO_2 Capture Adsorbent in View of Regeneration Strategies. *Ind. Eng. Chem. Res.* **2017**, *56*, 3259–3269. [CrossRef]
44. Chaikittisilp, W.; Kim, H.J.; Jones, C.W. Mesoporous alumina-supported amines as potential steam-stable adsorbents for capturing CO_2 from simulated flue gas and ambient air. *Energy Fuels* **2011**, *25*, 5528–5537. [CrossRef]
45. Chaikittisilp, W.; Khunsupat, R.; Chen, T.T.; Jones, C.W. Poly(allylamine)–Mesoporous Silica Composite Materials for CO_2 Capture from Simulated Flue Gas or Ambient Air. *Ind. Eng. Chem. Res.* **2011**, *50*, 14203–14210. [CrossRef]
46. Veneman, R.; Hilbers, T.; Brilman, D.W.F.; Kersten, S.R.A. CO_2 capture in a continuous gas–solid trickle flow reactor. *Chem. Eng. J.* **2016**, *289*, 191–202. [CrossRef]
47. Gebald, C.; Wurzbacher, J.A.; Tingaut, P.; Zimmermann, T.; Steinfeld, A. Amine-Based Nanofibrillated Cellulose As Adsorbent for CO_2 Capture from Air. *Environ. Sci. Technol.* **2011**, *45*, 9101–9108. [CrossRef]
48. Moulijn, J.A.; Makkee, M.; van Diepen, A. *Chemical Process Technology*; John Wiley & Sons: Hoboken, NJ, USA, 2001; ISBN 9780471630098.
49. Veneman, R.; Frigka, N.; Zhao, W.; Li, Z.; Kersten, S.; Brilman, W. Adsorption of H_2O and CO_2 on supported amine sorbents. *Int. J. Greenh. Gas Control* **2015**, *41*, 268–275. [CrossRef]
50. Long, W.; Xu, J.; Fan, Y.; Lu, C. Pinning and cavity in two types of cross-flow moving beds. *Powder Technol.* **2015**, *269*, 66–74. [CrossRef]
51. Song, X.; Jin, Y.; Yu, Z. Influence of outward radial gas flow on particle movement in an annular moving bed. *Powder Technol.* **1994**, *79*, 247–256. [CrossRef]
52. Choi, S.; Gray, M.L.; Jones, C.W. Amine-tethered solid adsorbents coupling high adsorption capacity and regenerability for CO_2 capture from ambient air. *ChemSusChem* **2011**, *4*, 628–635. [CrossRef]
53. Sinha, A.; Darunte, L.A.; Jones, C.W.; Realff, M.J.; Kawajiri, Y. Systems Design and Economic Analysis of Direct Air Capture of CO_2 through Temperature Vacuum Swing Adsorption Using MIL-101(Cr)-PEI-800 and mmen-Mg_2(dobpdc) MOF Adsorbents. *Ind. Eng. Chem. Res.* **2017**, *56*, 750–764. [CrossRef]